

Anomalous thermal transport in MgSe with diamond phase under pressureWei Cao,¹ Jing Shi,² Rui Xiong,² Ling Miao,³ Ziyu Wang^{1,*} and Zhengyou Liu²¹*The Institute of Technological Sciences, Wuhan University, Wuhan 430072, People's Republic of China*²*Key Laboratory of Artificial Micro- and Nano-structures of Ministry of Education, School of Physics and Technology, Wuhan University, Wuhan 430072, People's Republic of China*³*School of Optical and Electronic Information, Huazhong University of Science and Technology, Wuhan 430074, People's Republic of China*

(Received 5 March 2023; revised 17 May 2023; accepted 23 May 2023; published 7 June 2023)

Most materials exhibit a monotonically increasing lattice thermal conductivity with pressure. However, in this work, we report anomalous thermal transport properties of MgSe with a diamond phase under high pressure by first-principles calculations. Unlike other selenides, the lattice thermal conductivity of MgSe decreases with increasing pressure. We attribute this anomalous thermal transport to both harmonic and anharmonic effects. The harmonic effect is related to the anomalous downward shift of the transverse acoustic modes, which leads to decreasing phonon group velocities. This anomalous harmonic effect can also be confirmed by anomalous soft elastic properties. The anharmonic effect, on the other hand, is related to the stronger anharmonic scattering strength under pressure. Through bonding analysis, we found that the alternating bonding and antibonding states, combined with the unique lattice structure, are the main reason behind this anomaly. Our results reveal that the abnormal soft elastic properties under pressure can be a new way to judge whether lattice thermal conductivity decreases with pressure.

DOI: [10.1103/PhysRevB.107.235201](https://doi.org/10.1103/PhysRevB.107.235201)**I. INTRODUCTION**

Thermoelectric materials are promising alternatives to solve the global energy crisis, as they can directly convert heat to electricity without any pollutants [1,2]. The thermoelectric efficiency of a material can be measured by its dimensionless figure of merit, ZT , which is defined as

$$ZT = S^2 \sigma T / (\kappa_e + \kappa_l), \quad (1)$$

where S is the Seebeck coefficient, σ is the electrical conductivity, T is the absolute temperature, κ_e is the electronic thermal conductivity, and κ_l is the lattice thermal conductivity [3,4]. Various approaches have been applied to enhance the thermoelectric properties [5–7]. Among these methods, applying high pressure or strain has proved to be effective in increasing the thermoelectric properties [8]. However, κ_l usually increases with pressure, which greatly limits the effect of increasing thermoelectric properties by applying pressure. If κ_l can be unchanged or reduced with pressure, it is expected that decoupling and regulation of thermoelectric properties through pressure can be achieved.

As early as 1924, Bridgman [9] measured the law of thermal conductivity with pressure and drew relevant conclusions. Liebfried and Schlömann (LS) [10] further summarized the LS theory on the results. In LS theory, κ_l can be expressed as:

$$\kappa_l = \frac{AV^{1/3}\theta^3}{\gamma^2 T}, \quad (2)$$

where A is a constant, V is the volume, θ is the Debye frequency, and γ is the weighted average Grüneisen parameter. According to LS theory, the κ_l of nonmetallic crystal materials always increases with increasing pressure P ($d\kappa_l/dP > 0$). However, LS theory is a simplified approximation based on existing experimental results and cannot be applied to all systems. Using first-principles calculations, Parrish *et al.* [11] found that the thermal conductivity of silicon is constant when compressed and only begins to decrease when the system is stretched. This result contradicts previous classical molecular dynamic simulation results [12]. Hohensee *et al.* [13] also observed this unique thermal transport behavior of silicon before the phase transition. It should be noted that the anomalous pressure dependence of κ_l often occurs in phase transition materials. This work does not discuss any phase transition materials.

Currently, research on special thermal transport properties under pressure is primarily focused on theoretical calculations. Lindsay *et al.* [14] calculated the κ_l of binary compound materials under pressure and demonstrated that the κ_l decreases with increasing pressure for compounds with a large mass ratio. They believed that this anomalous pressure dependence of κ_l was due to the intrinsic scattering processes for heat-carrying acoustic phonons. Ouyang and Hu [15] reported that the anomalous pressure dependence of κ_l in tellurides depended on the competition between the increase in the velocity of longitudinal acoustic (LA) and optical phononic modes, and the decrease in phonon relaxation time in transverse acoustic (TA) phononic modes. Ravichandran and Broido [16] found a nonmonotonic relationship between κ_l and pressure in boron arsenide, revealing the competitive response of three-phonon scattering and four-phonon

*zywang@whu.edu.cn

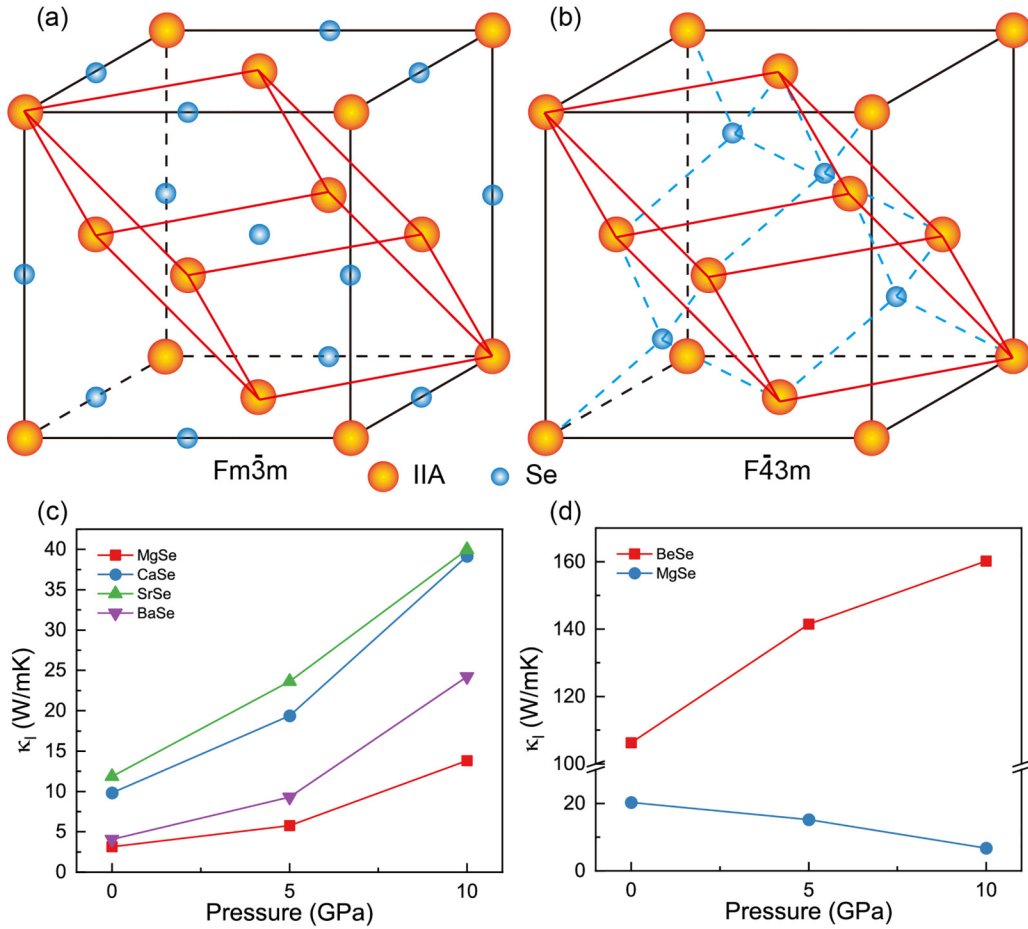


FIG. 1. The crystal structure of (a) $Fm\bar{3}m$ and (b) $F\bar{4}3m$ space groups. The primitive cell is marked by red lines. The κ_l of (c) $Fm\bar{3}m$ and (d) $F\bar{4}3m$ space group structures as a function of pressure.

scattering with pressure in boron arsenide. After that, Ravichandran and Broido [17] also found that the κ_l of boron phosphide first increases, and then decreases with increasing pressure, revealing the hidden effect of the weak three-phonon scattering channel generated by the selection rule on anharmonic decay. A recent experimental study [18] observed an anomalous pressure dependence of the κ_l in boron arsenide, resulting from competing three-phonon and four-phonon scattering processes.

The mechanisms explaining the anomalous pressure dependence of κ_l in the literature are different and cannot be applied universally. These materials usually have a high κ_l , indicating unsatisfactory thermoelectric properties. However, as discussed in Ref. [14], binary compounds composed of IIA and VIA elements show anomalous behavior between pressure and κ_l . Moreover, selenides are promising low-cost and environmentally benign thermoelectric materials [19]. Taking this into consideration, we selected IISe (where II represents the IIA group elements, including beryllium, magnesium, calcium, strontium, and barium) to explore materials with anomalous pressure dependence of κ_l .

II. COMPUTATIONAL METHODS

First-principles calculations are completed using the Vienna Ab initio Simulation Package (VASP) [20] via the

projector augmented-wave approach. The Perdew-Burke-Ernzerhof is adopted for the exchange and correlation functions [21]. The kinetic energy cut is set as 500 eV, and the lattice density of the Brillouin zone is $12 \times 12 \times 12$. The convergence criteria for energy and force are 10^{-8} eV and 10^{-3} eV \AA^{-1} , respectively. The calculation of elastic parameters and deformation charge density was computed using VASPKIT [22]. The deformation charge density was visualized with VESTA [23] software. The LOBSTER [24,25] package was used to calculate the projected crystal orbital Hamilton population (COHP).

The κ_l was calculated by using the phonon Boltzmann transport equation, which was expressed as

$$\kappa_l = \frac{1}{3VN_q} \sum_{q\gamma} C_{q\gamma} v_{q\gamma}^2 \tau_{q\gamma}, \quad (3)$$

where V is the volume of the unit cell, γ is the phonon mode index, q is the wave vector, N_q is the number of discrete k -points, $C_{q\gamma}$ is the heat capacity, $v_{q\gamma}$ is the group velocity, and $\tau_{q\gamma}$ is the phonon relaxation time. This can be done by using the ShengBTE [26] package, which requires harmonic (second) and anharmonic (third) interatomic force constants (IFCs) as inputs. To reduce the amount of calculation, the results in Figs. 1(c) and 1(d) were calculated by fitting IFCs as implemented in the HiPhive [27] code. This method has been

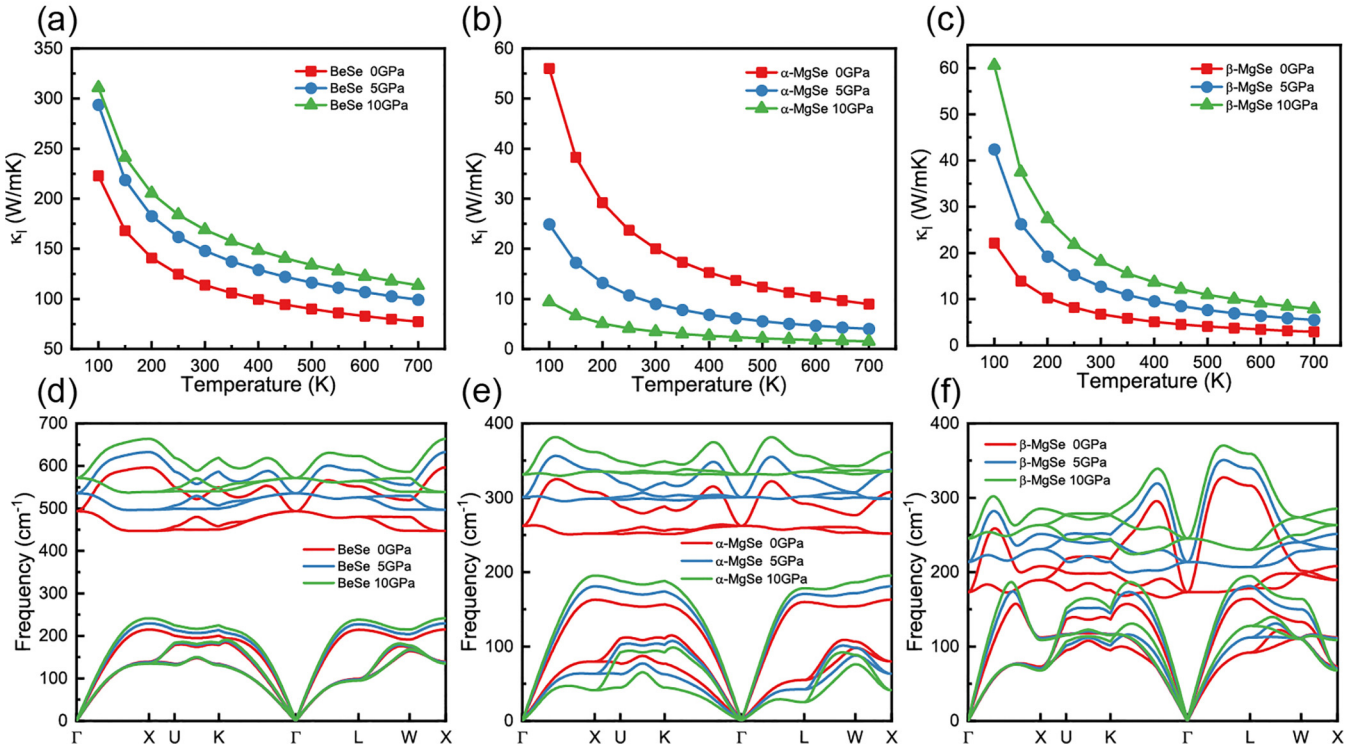


FIG. 2. The κ_l of (a) BeSe, (b) α -MgSe, and (c) β -MgSe under different pressures as a function of temperature. The phonon dispersion of (d) BeSe, (e) α -MgSe, and (f) β -MgSe under different pressures.

proved to have the same accuracy as traditional first-principles calculations and is tens of times less time-consuming [28,29]. Details about fitting IFCs can be found in the Supplemental Material Table S2 [30]. In order to obtain more accurate phonon properties [as shown in Figs. 2(a)–2(c)], the supercells selected for calculating the second and third IFCs were $5 \times 5 \times 5$ and contain 250 atoms. The second and third IFCs were calculated using the PHONOPY [31] package and thirddorder.py code [26], respectively. The tenth nearest neighbors were chosen as the interaction cutoff for the third IFCs. The phonon grid is set to $30 \times 30 \times 30$ and the smearing parameter is set to 0.1. The convergence test for the phonon grid and smearing parameter can be found in the Supplemental Material Fig. S2 [30].

III. RESULTS AND DISCUSSION

First, we screened cubic ISe binary compounds using the Materials Project database [32]. The space group for cubic ISe includes $F\bar{4}3m$ and $Fm\bar{3}m$, as shown in Figs. 1(a) and 1(b). We tested the structural stability of these ISe binary compounds and found that BeSe ($Fm\bar{3}m$), SrSe ($F\bar{4}3m$), and BaSe ($F\bar{4}3m$) cannot exist stably. Although CaSe ($F\bar{4}3m$) can exist stably, there are large imaginary frequencies in the phonon dispersion when a pressure of 2 GPa is applied, as shown in the Supplemental Material Fig. S1 [30]. Therefore, we will ignore CaSe ($F\bar{4}3m$) in the following discussion.

Figures 1(c) and 1(d) shows the κ_l of ISe as a function of pressure, calculated by fitting IFCs. It is clear that the κ_l of ISe ($Fm\bar{3}m$) all increase with increasing pressure, while only MgSe ($F\bar{4}3m$) shows a decreasing κ_l with

increasing pressure. For the sake of comparison, we selected BeSe ($F\bar{4}3m$), MgSe ($F\bar{4}3m$), and MgSe ($Fm\bar{3}m$) for further discussion. To simplify, we refer to MgSe ($F\bar{4}3m$) as α -MgSe, MgSe ($Fm\bar{3}m$) as β -MgSe, and the space group of BeSe defaults to $F\bar{4}3m$.

In Figs. 2(a)–2(c), we present κ_l as a function of temperature for three selenides under different pressures. Due to the intrinsic phonon scattering enhancement, κ_l for these selenides decreases with increasing temperature from 100 to 700 K. For the case without pressure, the order of κ_l for these selenides is BeSe > α -MgSe > β -MgSe. For instance, at room temperature, κ_l of BeSe, α -MgSe, and β -MgSe are 113.8 W/mK, 20 W/mK, and 6.7 W/mK, respectively. It is noteworthy that κ_l of α -MgSe decreases with increasing pressure. For instance, κ_l of α -MgSe at room temperature is 20 W/mK, and it decreases to 9 W/mK when a pressure of 5 GPa is applied. Furthermore, when the pressure continues to increase to 10 GPa, κ_l of α -MgSe decreases to 3.4 W/mK. The κ_l of α -MgSe can drop as low as 1.5 W/mK under 10 GPa at 700 K, which makes α -MgSe an ideal candidate for thermoelectric applications. The results of BeSe and β -MgSe are consistent with conventional crystal structures, where κ_l increases with increasing pressure.

According to the results in Ref. [14], the anomalous pressure dependence of κ_l is more likely to occur with a large mass ratio. Although the mass ratio of BeSe is greater than that of MgSe, this anomalous phenomenon does not occur in BeSe. Therefore, mass ratio is not the criterion in this work. In addition, α -MgSe and β -MgSe have the same elemental composition, but the κ_l of α -MgSe and β -MgSe shows different trends with pressure, indicating that lattice structure also plays an important role.

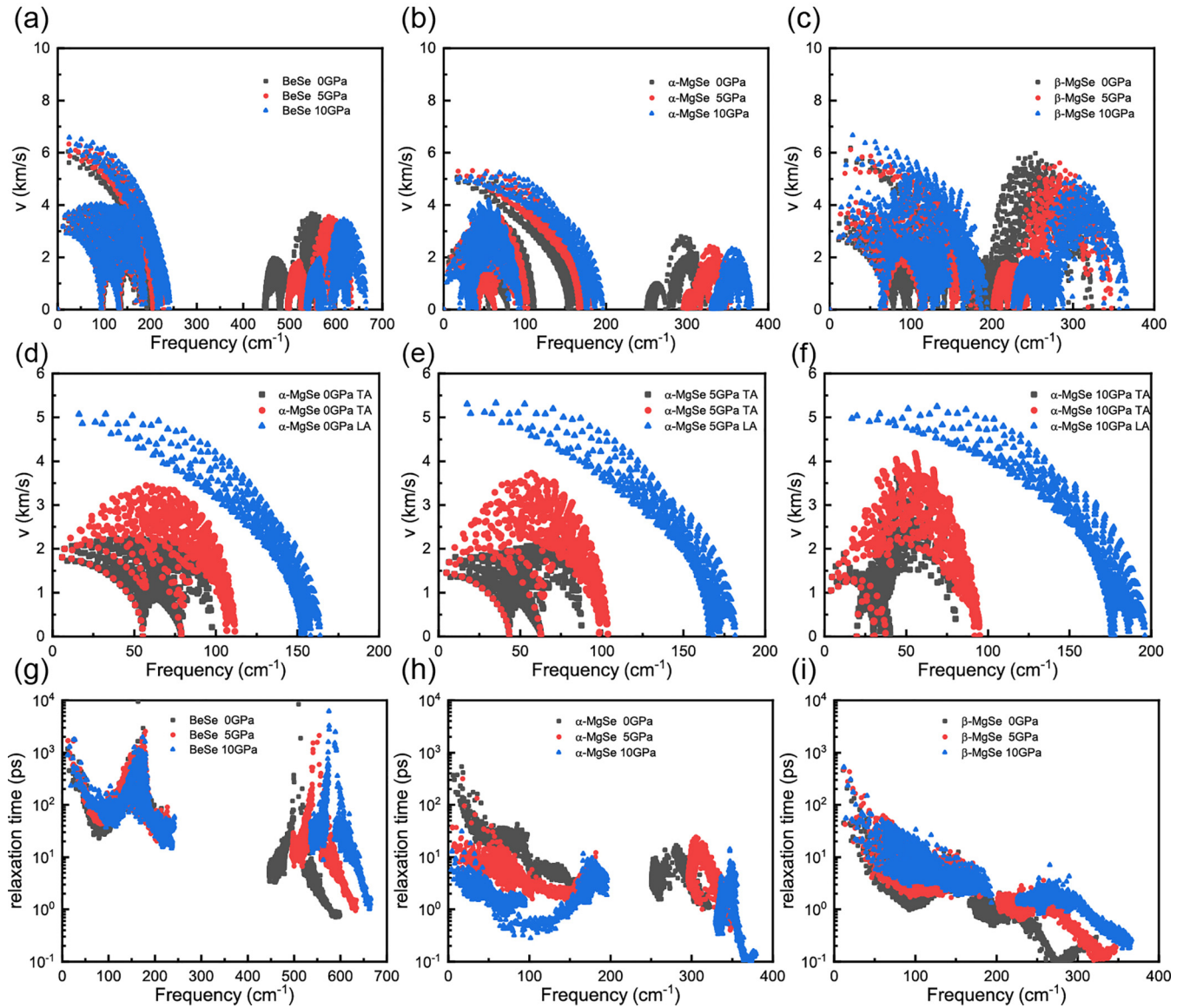


FIG. 3. The phonon group velocity of (a) BeSe, (b) α -MgSe, and (c) β -MgSe at different pressures. The group velocities for acoustic phonon modes of α -MgSe are given at pressures of (d) 0 GPa, (e) 5 GPa, and (f) 10 GPa. The phonon relaxation time of (g) BeSe, (h) α -MgSe, and (i) β -MgSe at different pressures.

To analyze the intrinsic mechanisms of this anomalous phenomenon further, we present the phonon dispersions of three structures at different pressures in Figs. 2(d)–2(f). After applying pressure, there are no imaginary frequencies in these phonon dispersions, indicating that these three structures are stable under pressures ranging from 0 to 10 GPa. Comparing the phonon dispersions of the three structures, it is found that BeSe and α -MgSe exhibit wide phonon bandgaps, while the phonon bandgap of β -MgSe is much narrower. The phonon bandgaps of the three structures increase with increasing pressure. The larger the bandgap between the optical and acoustic branches, the weaker the interaction between acoustic modes and optical modes, the weaker the phonon scattering, and thus the higher the κ_l . The optical modes move to higher frequencies with increasing pressure. Interestingly, it is found that the two TA modes of α -MgSe move downward with pressure, while the two TA modes of the other struc-

tures remain unchanged. Therefore, we believe that the two TA modes of α -MgSe moving downward with pressure are the main cause of the anomalous pressure dependence of κ_l .

To reveal the underlying mechanism, we discuss additional phononic parameters under varying pressures. In Figs. 3(a)–3(c), we present the phonon group velocities of three structures at different pressures and a temperature of 300 K. It can be seen that the phonon group velocities for BeSe, α -MgSe, and β -MgSe are relatively similar, with a maximum group velocity of 6 km/s. The group velocities of optical modes in BeSe and α -MgSe are significantly lower than those of acoustic modes, while the group velocities of optical modes in β -MgSe are comparable to those of acoustic modes. This is consistent with the previous phonon dispersions, where the optical branches of β -MgSe from Γ to other points appear very steep. However, the phonon group velocity of the three structures has not changed significantly,

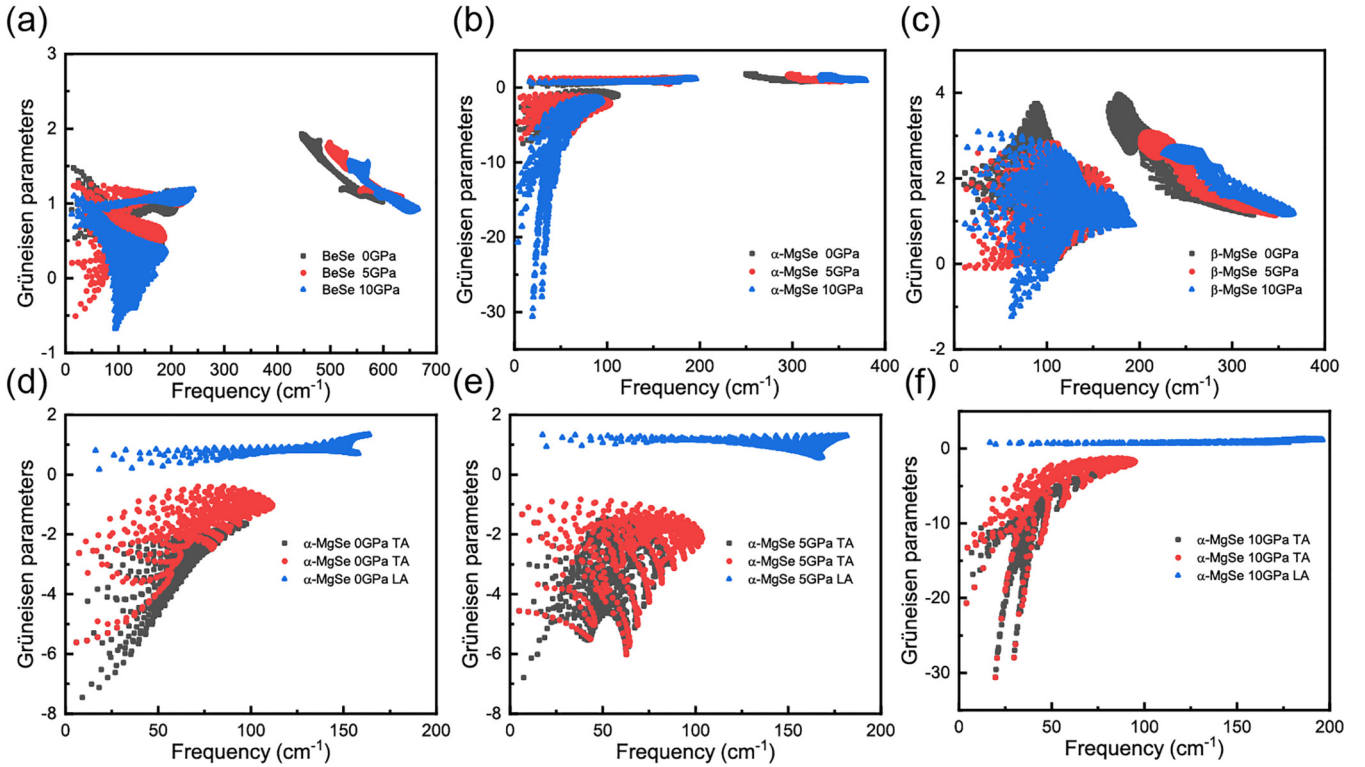


FIG. 4. The Grüneisen parameters of (a) BeSe, (b) α -MgSe, and (c) β -MgSe at different pressures. The Grüneisen parameters for acoustic phonon modes of α -MgSe at pressure of (d) 0 GPa, (e) 5 GPa, and (f) 10 GPa.

indicating that phonon group velocity is not the main determinant of κ_l . Furthermore, we examine the group velocities of different modes for α -MgSe, as illustrated in Figs. 3(d)–3(f). The group velocities for the LA mode peak at approximately 5 km/s under different pressures. However, the group velocities for the TA modes, especially the low-frequency portion ($< 50 \text{ cm}^{-1}$), decrease with increasing pressure. For example, at the Γ -point (around 0 cm^{-1}), the group velocities for TA modes are 2 km/s, 1.5 km/s, and 1 km/s for pressures of 0 GPa, 5 GPa, and 10 GPa, respectively. The anomalous downward shift of the TA modes leads to lower group velocities for TA modes in α -MgSe. A recent work [33] reported that the elastic behavior of a material can be a powerful tool for deciphering thermal transport. The group velocities for LA and TA modes can reflect the longitudinal and shear sound velocity, which are linked to lower elastic moduli.

In Figs. 3(g)–3(i), we present the phonon relaxation time of three structures under different pressures at 300 K. The shift in phonon relaxation time with pressure behaves similarly to phonon group velocity. However, the phonon relaxation time of BeSe and β -MgSe gradually increases with pressure, while the phonon relaxation time of α -MgSe gradually decreases with pressure. Figure 3(h) shows that the phonon relaxation time in the low frequency, which corresponds to the acoustic modes, decreases significantly with increasing pressure. The phonon relaxation time of optical modes in α -MgSe is also significantly reduced, but the contribution of high-frequency phonons to κ_l is limited. The anomalous pressure dependence of κ_l is mainly due to the phonon relaxation time of acoustic modes. This relaxation time is primarily related to the square of the Grüneisen parameter (the

strength of anharmonic scattering) and the P_3 parameter (the number of anharmonic scattering channels) [34]. The Supplemental Material Fig. S4 [30] provides the P_3 parameters, which remained relatively constant with pressure. Therefore, we focus on the Grüneisen parameters in the following discussion.

In Figures 4(a)–4(c), we present the Grüneisen parameters for three structures at 300 K and different pressures. α -MgSe's acoustic modes have negative Grüneisen parameters, and their absolute values increase with pressure, indicating stronger anharmonic scattering strength. This stronger anharmonicity leads to a lower κ_l , which partially explains the results. BeSe and β -MgSe's Grüneisen parameters do not change significantly with pressure. We observe that the Grüneisen parameter of α -MgSe is particularly reduced for the TA modes. In Figs. 4(d)–4(f), we display the Grüneisen parameter and pressure change corresponding to the three acoustic modes of α -MgSe. We see that the Grüneisen parameter of LA modes changes less with pressure, while the Grüneisen parameters for TA modes decrease significantly with pressure. At 0 GPa, the Grüneisen parameter of TA is primarily around -2 , but when the pressure reaches 12 GPa, the Grüneisen parameter of TA is mainly around -10 , with a minimum value reaching -30 , especially for the lower frequency part.

Figure 5 displays the growth ratio of the second IFCs and the lattice constant. Higher second IFCs correspond to stronger bonding. α -MgSe exhibits an ultraflat growth ratio of second IFCs, but also displays a large reduction in the lattice constant compared to BeSe and β -MgSe. When pressure is applied, the volume of α -MgSe can easily decrease due to

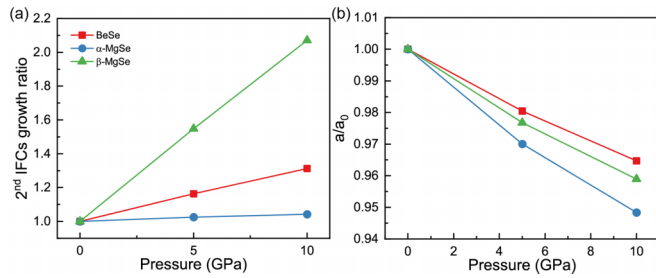


FIG. 5. Growth ratio of (a) second IFCs and (b) the lattice constant as a function of pressure.

its weak bonding. More specifically, under the same pressure, the structure of α -MgSe is softer and easier to compress into a smaller volume. Soft bonding can lead to more significant atomic displacement during vibration. Therefore, the weak bonding also leads to stronger anharmonic interactions and larger absolute values of Grüneisen parameters.

To gain a deeper understanding of anomalous mechanisms in α -MgSe, we present the projected COHP in Figs. 6(a)–6(c). Negative and positive COHP values correspond to bonding and antibonding characters, respectively. After applying pressure, the shapes of COHP for all structures did not change, but they shifted slightly toward a lower energy level as a whole. Applying pressure does not alter the essential bonding state.

Under the Fermi level, the COHP of BeSe is all negative, indicating strong bonding characters. Interestingly, the COHP of α -MgSe and β -MgSe under the Fermi level are composed of alternating bonding and antibonding states. This leads to much weaker bonding states than in BeSe, which is also reflected by the absolute values of COHP. However, β -MgSe does not show anomalous thermal transport. We further exhibit the deformation charge density (DCD) of α -MgSe and β -MgSe in Figs. 6(d)–6(g). From the three-dimensional views in Figs. 6(d) and 6(e), the shapes of the DCD in α -MgSe and β -MgSe are similar due to the similar bonding and antibonding states in COHP. Because of the specific crystal symmetry of $Fm\bar{3}m$, the selenium atom in β -MgSe is surrounded by six magnesium atoms. The DCD in β -MgSe is coupled together and forms a circuit in Fig. 6(g). In contrast, the selenium atom in α -MgSe is surrounded by four magnesium atoms, and the DCD in α -MgSe is separated, as shown in Fig. 6(f). Although the basic bonding and antibonding characters in α -MgSe and β -MgSe are similar, the unique crystal symmetry in β -MgSe results in stronger bonding states than in α -MgSe. Thus, we attribute the anomalous thermal transport in α -MgSe to the alternating bonding and antibonding states in COHP and the diamond-like crystal symmetry.

The elastic properties of materials are widely used to evaluate the strength of interatomic bonding and lattice vibration anharmonicity. Figure 7 shows the elastic properties of the

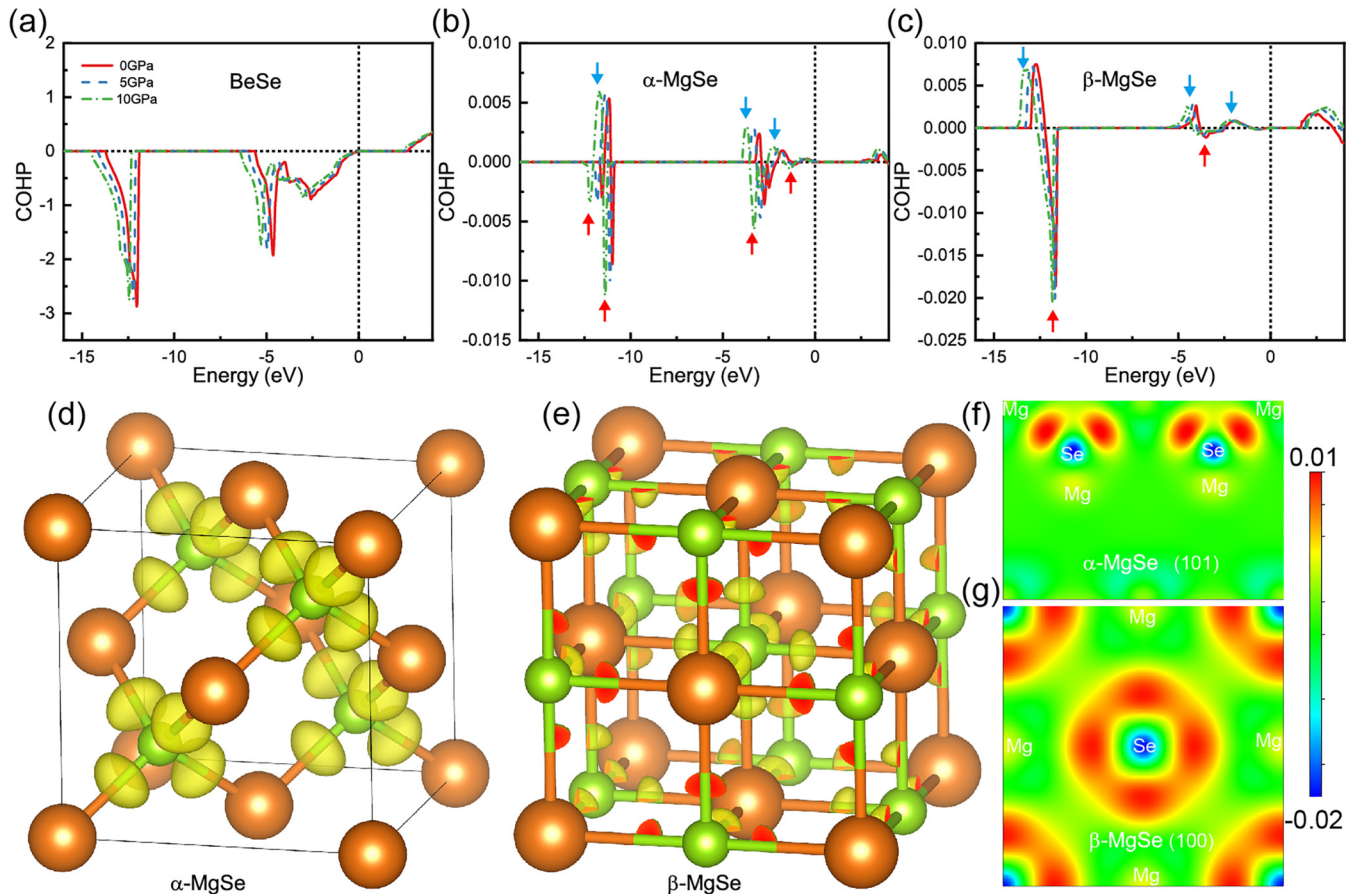


FIG. 6. The orbital-resolved projected crystal orbital Hamilton population (COHP) of (a) BeSe, (b) α -MgSe, and (c) β -MgSe under different pressures. Deformation charge density, given in units of electrons per cubic angstrom, for the (d) α -MgSe 3D, (e) β -MgSe 3D, (f) α -MgSe 2D, and (g) β -MgSe 2D views.

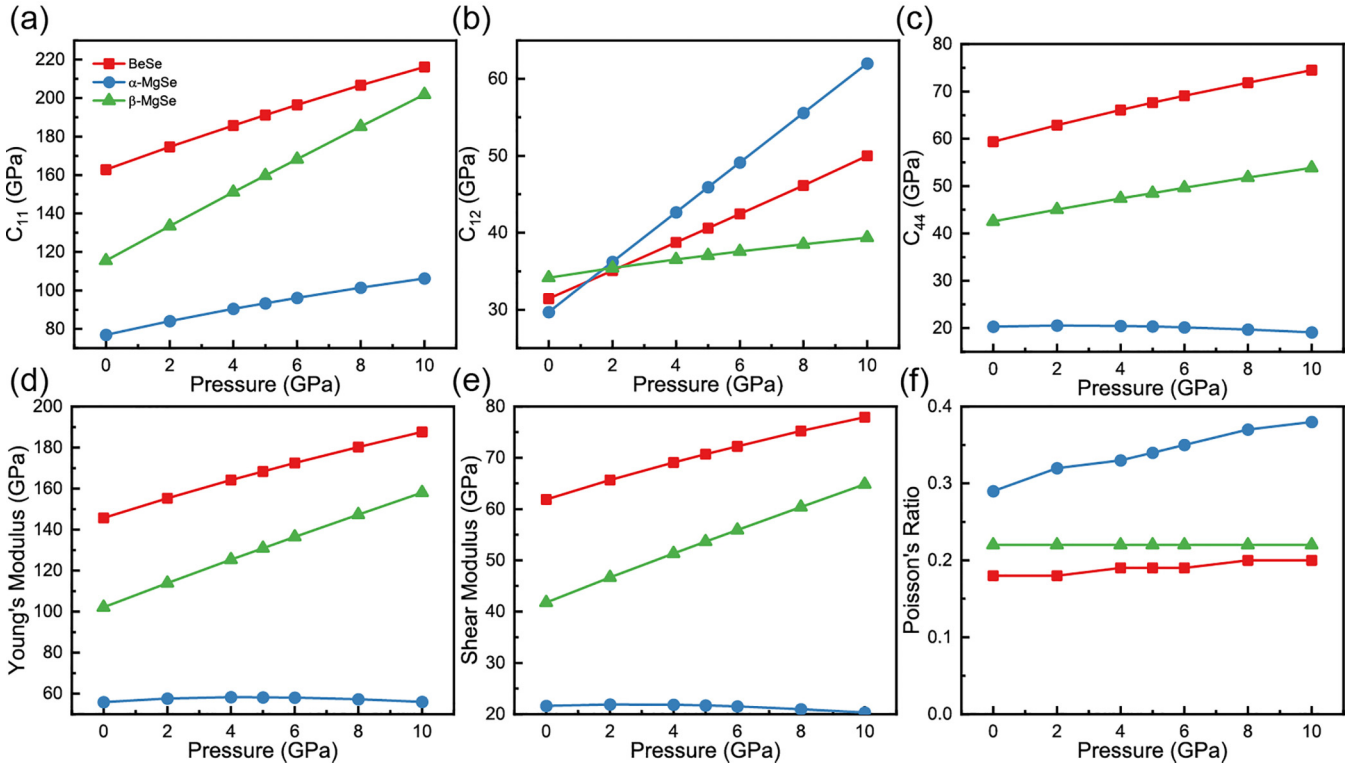


FIG. 7. The elastic properties of BeSe, α -MgSe, β -MgSe structures as a function of pressure: (a) C_{11} , (b) C_{12} , (c) C_{44} , (d) Young's modulus, (e) shear modulus, and (f) Poisson's ratio.

three structures as a function of pressure. We first analyze the C_{11} , C_{12} , and C_{44} parameters in the elastic constant matrix, as shown in Figs. 7(a)–7(c). These parameters represent stiffness in the direction of the stress, stiffness in response to a perpendicular stress, and stiffness in response to shear stress, respectively. For cubic crystals, the conditions of stability are simple: $C_{11} - C_{12} > 0$, $C_{11} + 2C_{12} > 0$; $C_{44} > 0$ [35]. The maximum values for C_{12} are much lower than the minimum values for C_{11} , which ensure stability for all structures under different pressures. Among the three structures, α -MgSe has lower slopes of C_{11} and C_{44} , and a higher lower slope of C_{12} . This indicates that α -MgSe has the strongest phonon anharmonicity. In addition, the change trend of the C_{44} parameter in α -MgSe reflects that the frequency of the TA modes will decrease under pressure. According to the definition of the Grüneisen parameter [36], if the frequency of the TA modes decreases with pressure, a negative Grüneisen parameter is caused, and the amplitude is determined by the slope of the decline of the C_{44} parameter.

As shown in Figs. 7(d) and 7(e), the slope of Young's modulus and shear modulus with pressure of α -MgSe is significantly lower than that of BeSe and β -MgSe. Generally, lower Young's modulus, shear modulus, and large Grüneisen parameters correspond to lower κ_l [37]. Furthermore, as displayed in Fig. 7(f), the slope of the Poisson's ratio of α -MgSe is significantly higher than that of BeSe and β -MgSe. Weaker bond strength results in softer phonon models and stronger phonon vibrations during thermal transport. These elastic results indicate that the anomalous changes in Young's modulus, shear modulus, and Grüneisen parameters in α -MgSe with

pressure are due to the soft bonds, which is the fundamental reason for the anomalous change in κ_l . The mechanical properties under pressure can be used to determine whether there will be anomalous changes in κ_l .

IV. CONCLUSION

In this work, we investigate the effects of pressure on the lattice thermal conductivity of the α -MgSe (diamond-phase) lattice. Unlike conventional crystalline materials, the lattice thermal conductivity of α -MgSe decreases with increasing pressure. To analyze the intrinsic causes, we compared BeSe (diamond phase, the same structure) and β -MgSe (NaCl phase, the same composition), and showed that only α -MgSe exhibited this anomalous change in lattice thermal conductivity. Bonding analysis revealed that α -MgSe and β -MgSe exhibit alternating bonding and antibonding states. However, the selenium atom in β -MgSe is surrounded by six magnesium atoms and forms a coupled, strong bonding state. Bonding states in α -MgSe are separate and remain weak, which leads to a stronger anharmonic scattering strength. The transverse acoustic modes abnormally move to lower frequencies, leading to decreasing phonon group velocities. These lower phonon group velocities cause soft elastic properties. The abnormal soft elastic properties under pressure can be another way to reflect the abnormal thermal transport.

ACKNOWLEDGMENTS

The authors acknowledge the financial support of the project from the National Key R&D Program of China

(Grant No. 2021YFA0718700), the National Natural Science Foundation of China (Grants No. 12122408, No. 12074292, and No. 91963207), and the Hubei Provincial Natural

Science Fund for Distinguished Young Scholars (Grant No. 2019CFA083).

-
- [1] X. Shi and L. Chen, *Nat. Mater.* **15**, 691 (2016).
- [2] G. Tan, L.-D. Zhao, and M. G. Kanatzidis, *Chem. Rev.* **116**, 12123 (2016).
- [3] A. J. Minnich, M. S. Dresselhaus, Z. F. Ren, and G. Chen, *Energy Environ. Sci.* **2**, 466 (2009).
- [4] W. Liu, X. Yan, G. Chen, and Z. Ren, *Nano Energy* **1**, 42 (2012).
- [5] Y. Pei, X. Shi, A. LaLonde, H. Wang, L. Chen, and G. J. Snyder, *Nature (London)* **473**, 66 (2011).
- [6] J. P. Heremans, V. Jovovic, E. S. Toberer, A. Saramat, K. Kurosaki, A. Charoenphakdee, S. Yamanaka, and G. J. Snyder, *Science* **321**, 554 (2008).
- [7] T. C. Harman, P. J. Taylor, M. P. Walsh, and B. E. LaForge, *Science* **297**, 2229 (2002).
- [8] N. V. Morozova, I. V. Korobeinikov, and S. V. Ovsyannikov, *J. Appl. Phys.* **125**, 220901 (2019).
- [9] P. W. Bridgman, *Am. J. Sci.* **s5-7**, 81 (1924).
- [10] G. A. Slack, *Solid State Physics* (Academic, New York, 1979), Vol. 34, Chap. 3, pp. 1–71.
- [11] K. D. Parrish, A. Jain, J. M. Larkin, W. A. Saidi, and A. J. H. McGaughey, *Phys. Rev. B* **90**, 235201 (2014).
- [12] X. Li, K. Maute, M. L. Dunn, and R. Yang, *Phys. Rev. B* **81**, 245318 (2010).
- [13] G. T. Hohensee, M. R. Fellingner, D. R. Trinkle, and D. G. Cahill, *Phys. Rev. B* **91**, 205104 (2015).
- [14] L. Lindsay, D. A. Broido, J. Carrete, N. Mingo, and T. L. Reinecke, *Phys. Rev. B* **91**, 121202(R) (2015).
- [15] T. Ouyang and M. Hu, *Phys. Rev. B* **92**, 235204 (2015).
- [16] N. K. Ravichandran and D. Broido, *Nat. Commun.* **10**, 827 (2019).
- [17] N. K. Ravichandran and D. Broido, *Nat. Commun.* **12**, 3473 (2021).
- [18] S. Li, Z. Qin, H. Wu, M. Li, M. Kunz, A. Alatas, A. Kavner, and Y. Hu, *Nature (London)* **612**, 459 (2022).
- [19] T.-R. Wei, C.-F. Wu, F. Li, and J.-F. Li, *J. Materiomics* **4**, 304 (2018).
- [20] G. Kresse and J. Furthmüller, *Phys. Rev. B* **54**, 11169 (1996).
- [21] J. P. Perdew, K. Burke, and M. Ernzerhof, *Phys. Rev. Lett.* **77**, 3865 (1996).
- [22] V. Wang, N. Xu, J.-C. Liu, G. Tang, and W.-T. Geng, *Comput. Phys. Commun.* **267**, 108033 (2021).
- [23] K. Momma and F. Izumi, *J. Appl. Crystallogr.* **44**, 1272 (2011).
- [24] S. Maintz, V. L. Deringer, A. L. Tchougréeff, and R. Dronskowski, *J. Comput. Chem.* **37**, 1030 (2016).
- [25] S. Maintz, V. L. Deringer, A. L. Tchougréeff, and R. Dronskowski, *J. Comput. Chem.* **34**, 2557 (2013).
- [26] W. Li, J. Carrete, N. A. Katcho, and N. Mingo, *Comput. Phys. Commun.* **185**, 1747 (2014).
- [27] F. Eriksson, E. Fransson, and P. Erhart, *Adv. Theory Simul.* **2**, 1800184 (2019).
- [28] J. Brorsson, A. Hashemi, Z. Fan, E. Fransson, F. Eriksson, T. Ala-Nissila, A. V. Krasheninnikov, H.-P. Komsa, and P. Erhart, *Adv. Theory Simul.* **5**, 2100217 (2022).
- [29] J. J. Plata, V. Posligua, A. M. Márquez, J. Fernandez Sanz, and R. Grau-Crespo, *Chem. Mater.* **34**, 2833 (2022).
- [30] See Supplemental Material at <http://link.aps.org/supplemental/10.1103/PhysRevB.107.235201> for the structural stability test, details of fitting force constants, the thermal conductivity convergence test, the specific heat, the P_3 parameters, and the bulk modulus.
- [31] A. Togo and I. Tanaka, *Scr. Mater.* **108**, 1 (2015).
- [32] M. de Jong, W. Chen, T. Angsten, A. Jain, R. Notestine, A. Gamst, M. Sluiter, C. Krishna Ande, S. van der Zwaag, J. J. Plata, C. Toher, S. Curtarolo, G. Ceder, K. A. Persson, M. Asta, *Sci. Data* **2**, 150009 (2015).
- [33] E. Isotta, W. Peng, A. Balodhi, and A. Zevkink, *Angew. Chem. Int. Ed.* **62**, e202213649 (2023).
- [34] L. Lindsay and D. A. Broido, *J. Phys. Condens. Matter* **20**, 165209 (2008).
- [35] F. Mouhat and F.-X. Coudert, *Phys. Rev. B* **90**, 224104 (2014).
- [36] M. Blackman, *The Philosophical Magazine: A, J. Theory Exp. Appl. Phys.* **3**, 831 (1958).
- [37] H. Wang, E. Schechtel, Y. Pei, and G. J. Snyder, *Adv. Energy Mater.* **3**, 488 (2013).